

Development of a Wide Bandwidth Massive Eight Dissimilar Radiating Element Multiband MIMO Antenna for mm-Wave Application

Shrenik Suresh Sarade
Electronics Engineering
Walchand College of Engineering
Sangli, India
shreniks2k7@rediffmail.com

Sachin D. Ruikar
Electronics Engineering
Walchand College of Engineering
Sangli, India
sachin.ruikar@walchandsangli.ac.in

Received: 10 June 2022 | Revised: 26 July 2022 | Accepted: 28 July 2022

Abstract-This paper proposes a massive MIMO antenna operating on 6GHz frequency as millimeter-wave. It consists of eight dissimilar-shaped radiating elements. The radiating element of the antenna is designed using square shape with different cut slots. Parasitic elements and defected ground structure are introduced for the enhancement of the correlation coefficients and total active reflection coefficients of the MIMO antenna. The rectangular shape parasitic elements are placed between the square radiating patches. The ground plane consists of rectangular shape defected ground structures. The antenna is constructed on the FR-4 substrate. Parameters such as isolation, cross-correlation, and bandwidth are enhanced. The obtained through simulations antenna parameters values of return loss, isolation, cross-correlation, total active reflection coefficients, and bandwidth are less than -10dB, less than -9.30dB, less than 0.16, less than 0.00015, and greater than 200MHz respectively. The antenna operates on various bands with fractional bandwidth greater than 3% for a frequency of 6GHz. This antenna is useful for a variety of applications in wireless systems.

Keywords-MIMO; DGS; TARC; CC; ECC

I. INTRODUCTION

Antennas are a crucial part of communication systems. An antenna is used to transport data from one location to another without interfering with the original signal. As a result, there is a need to build an antenna that meets the requirements of the communication system, such as size, weight, and signal quality. Multiple Input and Multiple Output (MIMO) antennas play an important role in the antenna field nowadays. Multiple antennas may be present at the transmitter and the receiver. The low data rate in Single Input and Single Output (SISO) system can be improved using an MIMO antenna system. The data rate of MIMO antenna grows linearly and depends on the number of patches in the antenna. The performance of the MIMO antenna differs with return loss, isolation, correlation coefficients, and total active reflection coefficients. In a MIMO antenna, multiple radiating patches are positioned on the same substrate in close proximity to one another. The close proximity of the square radiating patches influences the isolation (which becomes high) between the radiating patches

and the correlation coefficients become higher. There is a requirement of improvement in antenna's isolation, correlation coefficients, and data rate. To improve isolation and correlation coefficients, several studies employ Defective Ground Structure (DGS), Parasitic Elements (PEs), metamaterials, Decoupling Structure (DS), and Electromagnetic Band Gap (EBG) approaches. A DGS technique is used to improve isolation. Cut slots of various shapes are used in the ground plane [1-6]. To improve isolation, a decoupling structure is constructed that decouples the input of radiating patches from the matching network setup in [7-11]. PEs are used to improve the isolation between the patches in [12-17]. From the above literature survey, it can be concluded that there is a requirement to develop a massive MIMO antenna that operates on wide bandwidth multiband applications, with better TARC and better cross correlation.

A diverse shaped-element gigantic MIMO antenna is proposed in this work. It operates at multiband frequency with wide band operation. Parasitic elements and a defective ground structure are used to improve antenna parameters such as isolation, cross correlation, and total active reflection coefficients.

II. DESIGN OF THE MASSIVE MIMO ANTENNA

The concept of the MIMO antenna is explained above along with the literature survey. In this section, the massive MIMO antenna is designed and explained in detail. The designed antenna comprises of 8 square radiating patches with distinct cut slots for the 6GHz frequency, as shown in Figure 1. The antenna dimensions are provided in Figure 2. The antenna is developed using a FR-4 substrate with 1.6mm height h and 4.4 dielectric constant. The antenna's geometrical structure, i.e. length L_{re} and width W_{re} , was created using the square radiating patch transmission line model [20], which has the dimensions listed in Table I, which shows the measurements of 8 radiating elements with varying cut slots. A rectangular cut slot [20] is placed in patch-1 and patch-3, with length C and width D . A similar rectangular cut slot [20] is placed in patches-5, -7, and -8. A square cut slot is placed in patch-6, with both length and

Corresponding author: Shrenik Suresh Sarade

width C. The cut slot dimensions of the single patch are optimized using the equivalent circuit explained in Section III. Inset Feed Line (IFL) [20] with length C and width D is used to excite the antenna elements (dimensions listed in Table I). The

antenna's dimensions (FR-4 substrate) which consist of length E and width F of the patch are summarized in Table I. The distance between the parasitic elements and the radiating patches is less than half of the wavelength.

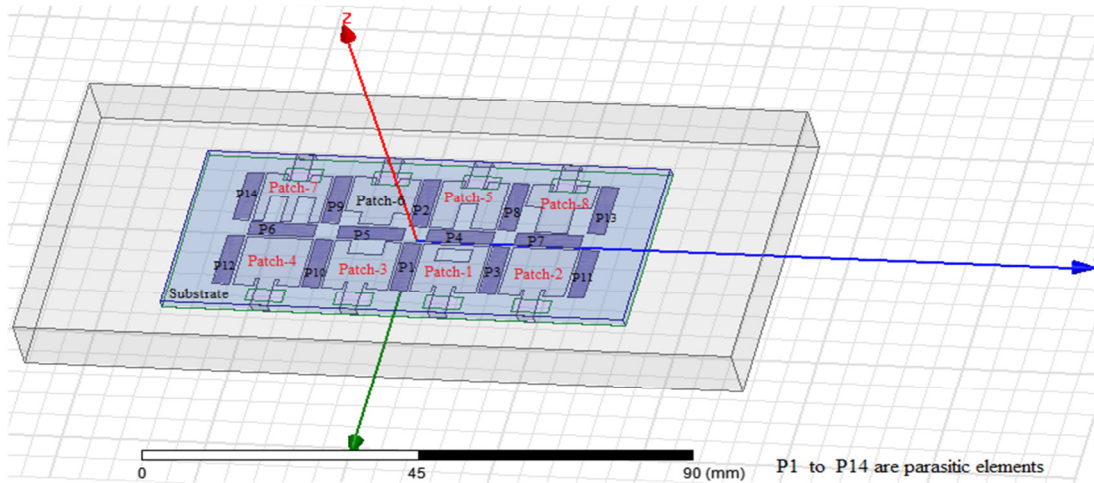


Fig. 1. Massive MIMO antenna with 8 distinct shaped components with PEs and a GDS.

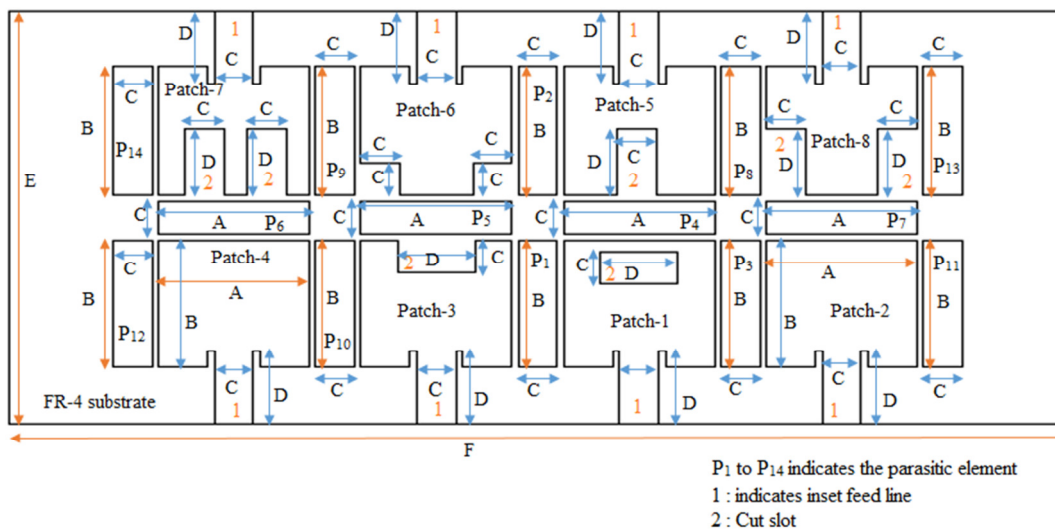


Fig. 2. The dimensions of the developed massive MIMO antenna.

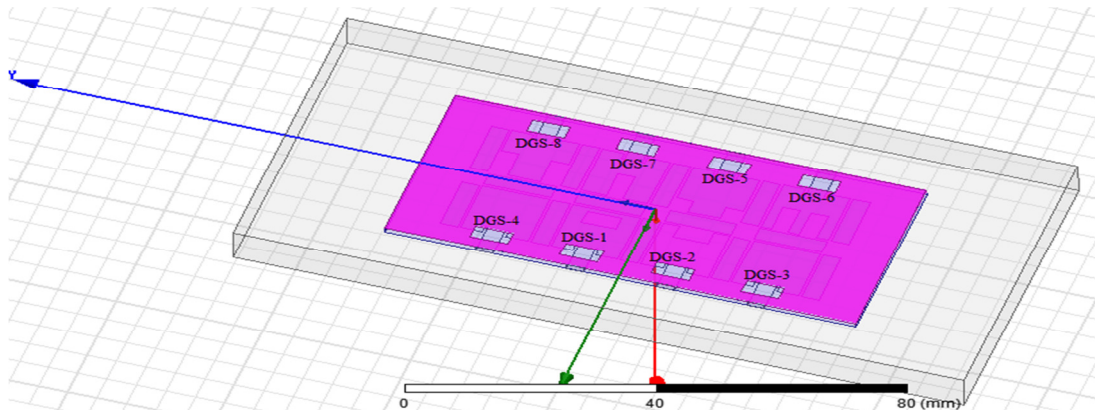


Fig. 3. The ground plane of antenna with DGS.

PEs and DGS improve the Total Active Reflection Coefficients (TARC), the Correlation Coefficient (CC), and the Envelope Correlation Coefficient (ECC) values between the radiating elements. Table I shows the size of parasitic elements (P1 to P14) [12-17]. As indicated in Figure 1, rectangular shaped Parasitic Elements (PEs) are used between the radiating patches. The PEs are used to negate parts of the coupled field between the elements because it creates an opposite coupling field, which lessens the original field and hence reduces total coupling on the antenna. The PE structure and the radiating patch are not physically related. Figure 3 depicts the antenna's ground plane, while Figure 4 depicts its dimensions. Table I shows the length D and width C of the DGS in the ground plane. The ground plane is made up of rectangular-DGS cut slots [1-6] that are utilized to improve isolation

TABLE I. ANTENNA DIMENSIONS

Sr. no.	Parameter	Dimensions (in mm)
1	Patch length (L_{re})	A = 11.38
2	Patch width (L_{re})	B = 11.38
3	Length of IFL	D = 6.41
4	Width of IFL	C = 2.942
5	Length of substrate	E = 36.522
6	Width of substrate	F = 80

III. EQUIVALENT CIRCUIT MODEL OF THE ANTENNA

In this section, the operation of the single radiating patch of the antenna is explained using the equivalent circuit model. That is applicable to all radiating patches. DGS and PEs are used in the development of the gigantic MIMO antenna. These two techniques are used to improve the antenna's isolation, TARC, CC, ECC, and bandwidth. The equivalent circuit mathematical model is used to describe how antennas work. The corresponding circuit of a single radiating patch is shown in Figure 5.

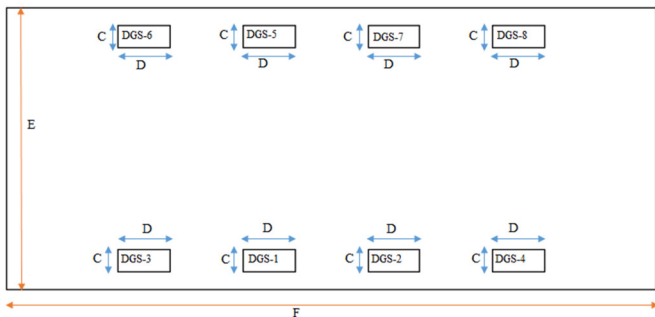


Fig. 4. The dimensions of the ground plane of the antenna with DGS.

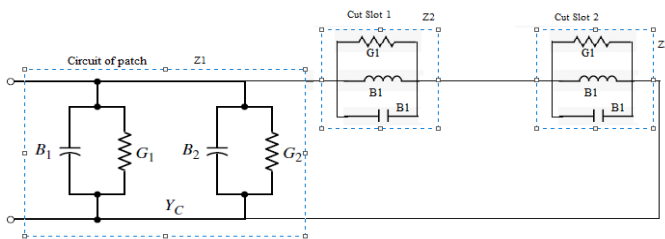


Fig. 5. Equivalent circuit model for square-radiating patch.

As shown in Figure 1, the antenna comprises of a square radiating patch with a cut slot. Figure 5 is divided into two parts: a square shape circuit with impedance Z_1 and rectangular cut slot-1 and 2 with impedance Z_2 and Z_3 . The inductor and capacitor values of the equivalent circuit [21] are used to compute the cut slot dimensions using (1) and (2):

$$G_1 = \frac{0.00833 W}{\lambda_0} [1 - 0.04167(k_0 H_{fr4})^2] \quad (1)$$

$$B_1 = \frac{0.00833 W}{\lambda_0} [1 - 0.636 \ln(k_0 H_{fr4})] \quad (2)$$

where G_1 is the resistive value of the circuit, B_1 is the capacitive or inductive value of the circuit, $W = L_{re}$ the width of the patch, h the height of the substrate, and k_0 constant.

Because the antenna elements have distinct cut slots, the antenna can function on many frequencies. This antenna's operating concept is similar to that of any other radiating patch, and cut slots are provided according to the desired frequency.

IV. RESULT ANALYSIS

The antenna is simulated using the High Frequency Structure Simulator (HFSS). Isolation, CC, ECC, TARC, and bandwidth [19] are the performance parameters of the MIMO antenna. The 8 radiating patches are arranged in a row (close to each other) which results in high level of isolation among the radiating patch. DGS and PE techniques are employed to improve the isolation between the radiating patches. The rectangular carved slit acts as a DGS in the ground. The DGS alters the properties of the transmission line's inductor and capacitor, resulting in a shift in the antenna's frequency response. A rectangular shaped PE is placed between the radiating elements to improve the antenna's isolation and bandwidth. It prevents the radiating energy passing from one element to the nearby element. The isolation performance between the parameters helps improve CC, ECC, and TARC.

The return loss (S_{11}) and the acquired isolation between the remaining elements of patch-1 are shown in Figure 6. The antenna operates on 6.2GHz (m_1) and 7.1GHz (m_3), with less than -17.50dB return loss (S_{11}), less than -11.25dB isolation (S_{12} (m_2 and m_4)), and 347.4MHz (5.79%) bandwidth. The isolation between the remaining patches, S_{13} , S_{14} , S_{15} , S_{16} , S_{17} , and S_{18} is less than -11.25dB (S_{12}).

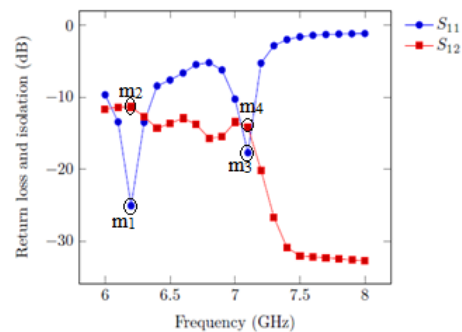


Fig. 6. Return loss (S_{11}) and isolation of patch-1.

The antenna element bandwidth [18-20] is obtained at -10dB return loss. The return loss (S_{22}) and the isolation

between the remaining elements of patch-2 are shown in Figure 7. It operates on the 5.7GHz, with less than -24.79dB return loss (S_{22} (m_1)), less than -11dB isolation (S_{26} (m_2)), and 437.3MHz (7.289%) bandwidth. The isolation between the remaining patches such as S_{21} , S_{23} , S_{24} , S_{25} , S_{27} , and S_{28} is less than -11dB (S_{26}).

The return loss (S_{33}) and the isolation between the remaining elements of patch-3 are shown in Figure 8. It operates on 5.8GHz (m_1) and 6.9GHz (m_3), with less than -12.50dB return loss (S_{33}), less than -11.40dB isolation (S_{34} (m_2) and m_4)), and 403.32 MHz (6.72%) bandwidth. The isolation between the remaining patches such as S_{31} , S_{32} , S_{35} , S_{36} , S_{37} , and S_{38} is less than -11.40dB (S_{34}).

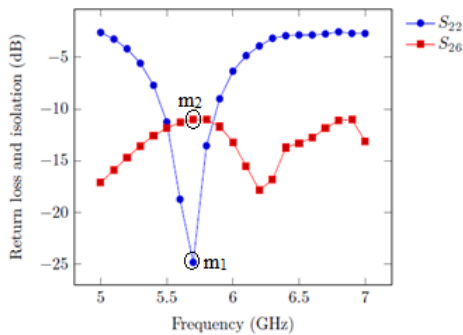


Fig. 7. Return loss (S_{22}) and isolation of patch-2.

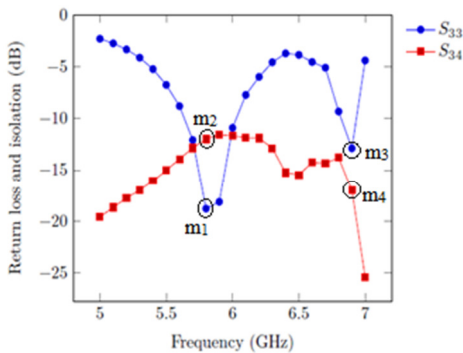


Fig. 8. Return loss (S_{33}) and isolation of patch-3.

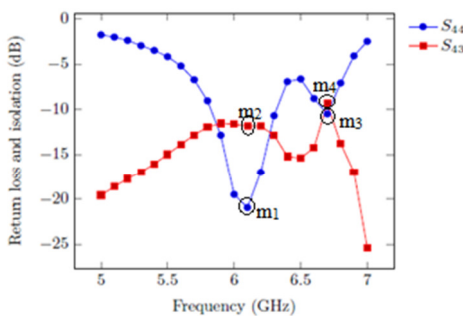


Fig. 9. Return loss (S_{44}) and isolation of patch-4.

The return loss (S_{44}) and the isolation between the remaining elements of patch-4 are shown in Figure 9. It operates on 6.1GHz (m_1) and 6.7GHz (m_3), with less than -10.25dB return loss (S_{44}), less than -9.35 dB isolation (S_{43} (m_2

and m_4)), and 488MHz (8.146%) bandwidth. The isolation between the remaining patches such as S_{41} , S_{42} , S_{45} , S_{46} , S_{47} , and S_{48} is less than -9.35 dB (S_{43}).

The return loss (S_{55}) and the isolation between the remaining elements of patch-5 are shown in Figure 10. It resonates on 5.8GHz (m_1) and 6.8GHz (m_3), with less than -18.50dB return loss (S_{55}), less than -9.70dB isolation (S_{51} (5.8GHz (m_2) and 5.8GHz (m_4))), and 399MHz (6.65%) bandwidth. The isolation between the remaining patches such as S_{52} , S_{53} , S_{54} , S_{56} , S_{57} , and S_{58} is less than -11.33dB (S_{51}).

The return loss (S_{66}) and the isolation between the remaining elements of patch-6 are shown in Figure 11. It resonates on 5.8GHz (m_1), with less than -20.92dB return loss (S_{66}), less than -11.17dB isolation (S_{67} (5.8GHz (m_2))), and 425.76 MHz (7.096%) bandwidth. The isolation between the remaining patches such as S_{61} , S_{62} , S_{63} , S_{64} , S_{65} , and S_{68} is less than -11.33dB (S_{67}).

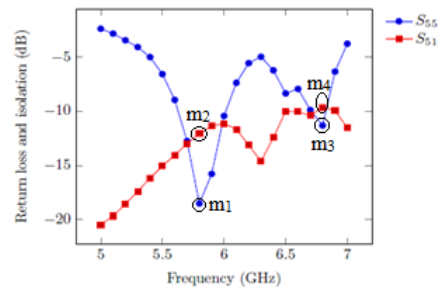


Fig. 10. Return loss (S_{55}) and isolation of patch-5.

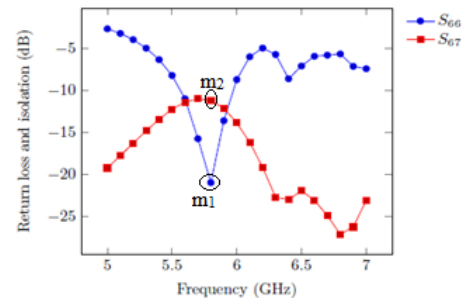


Fig. 11. Return loss (S_{66}) and isolation of patch-6.

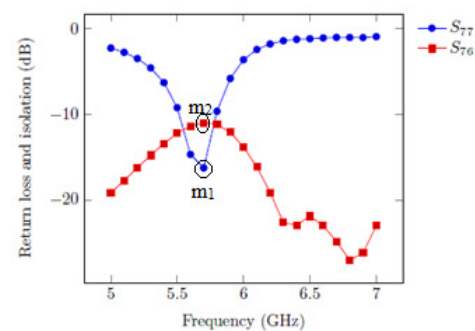


Fig. 12. Return loss (S_{77}) and isolation of patch-7.

The return loss (S_{77} (m_1)) and the isolation between the remaining elements of patch-7 are shown in Figure 12. It resonates at 5.7GHz, with less than -16.25dB return loss (S_{66}),

less than -10.98dB isolation ($S_{76}(m_2)$), and 297MHz (4.95%) bandwidth. The isolation between the remaining patches such as $S_{71}, S_{72}, S_{73}, S_{74}, S_{75}$, and S_{78} is less than -11.33dB (S_{76}).

The return loss (S_{88}) and the isolation between the remaining elements of patch-8 are shown in Figure 13. It resonates at 5.8GHz (m_1) and 6.8GHz (m_3), with less than -20.30dB return loss (S_{88}), less than -11.10dB isolation ($S_{84}(m_2$ and $m_4)$), and 379.2MHz (6.32%) bandwidth. The isolation between the remaining patches such as $S_{81}, S_{82}, S_{83}, S_{85}, S_{86}$, and S_{87} is less than -11.33dB isolation (S_{84}).

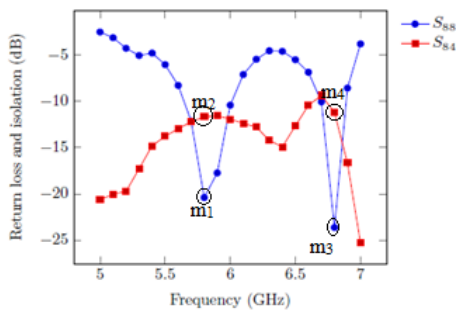


Fig. 13. Return loss (S_{88}) and isolation of patch-8.

The results of the antenna parameter investigation show that the gain attained is 2.69dB, as shown in Figure 14. Figure 15 shows the antenna radiation pattern. TARC is less than 0.16, CC is less than 0.0122, ECC is less than 0.00015, and DG is near to 9.9985 [20].

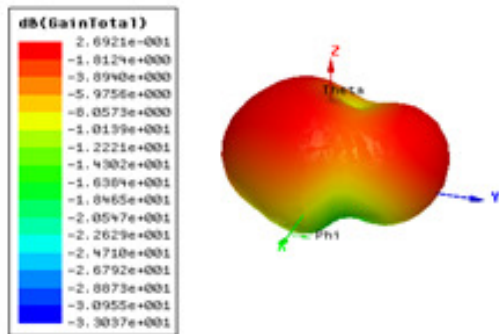


Fig. 14. Gain of the MIMO antenna.

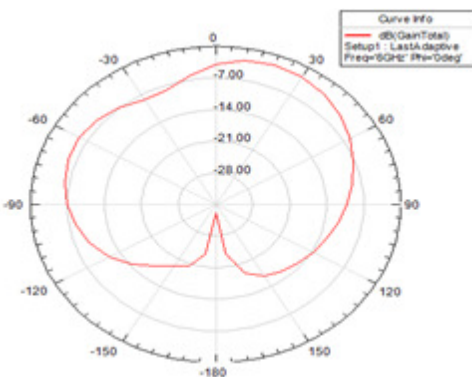


Fig. 15. Radiation pattern of the MIMO antenna.

V. COMPARISON

The proposed antenna's parameters are compared with other works in Table II. The comparison shows that the proposed antenna is developed for 8-different shaped radiating elements. It operates on the multiband frequency with a wide bandwidth.

TABLE II. COMPARISON OF THE PROPOSED ANTENNA WITH OTHER WORKS

Ref	Technique used	Parameter	Frequency band and bandwidth	Radiating patches
[1]	DGS	-10 dB RL, -12dB isolation	Single band and narrow band	Same shape 8-radiating patches
[7]	DGS	-20 dB RL, -15dB isolation	Dual band and narrow band	Same shape 8-radiating patches
[12]	PE	-10 dB RL, -10dB isolation	Dual band and wide band	Same shape 8-radiating patches
Proposed	DGS + PE	-10 dB RL, -9.30dB isolation	Multiband and wide band with better cross correlation	Different 8-shaped radiating patches

VI. CONCLUSION

The proposed 8 dissimilarized element antenna operates on various frequency bands for a wide bandwidth. The antenna parameters are enhanced using DGS and PEs. The proposed antenna operates at 5.7GHz, 5.8GHz, 6.1GHz, 6.2GHz, 6.7GHz, 6.8GHz, 6.9GHz, and 7.1GHz. The results obtained through simulations for various antenna parameter values show -10dB return loss, less than -9.30dB isolation, less than 0.16 CC, less than 0.0122 ECC, less than 0.00015 TARC, and bandwidth greater than 200MHz. The antenna operates on the various bands with fractional bandwidth greater than 3% for 6GHz frequency. This antenna is designed for various applications of communication systems with wide bandwidth operation.

REFERENCES

- [1] Y. Li, C.-Y.-D. Sim, Y. Luo, and G. Yang, "High-Isolation 3.5 GHz Eight-Antenna MIMO Array Using Balanced Open-Slot Antenna Element for 5G Smartphones," *IEEE Transactions on Antennas and Propagation*, vol. 67, no. 6, pp. 3820–3830, Jun. 2019, <https://doi.org/10.1109/TAP.2019.2902751>.
- [2] M. Y. Jamal, M. Li, and K. L. Yeung, "Isolation Enhancement of Closely Packed Dual Circularly Polarized MIMO Antenna Using Hybrid Technique," *IEEE Access*, vol. 8, pp. 11241–11247, 2020, <https://doi.org/10.1109/ACCESS.2020.2964902>.
- [3] W. Wang, Y. Wu, W. Wang, and Y. Yang, "Isolation Enhancement in Dual-Band Monopole Antenna for 5G Applications," *IEEE Transactions on Circuits and Systems II: Express Briefs*, vol. 68, no. 6, pp. 1867–1871, Jun. 2021, <https://doi.org/10.1109/TCSII.2020.3040164>.
- [4] J. C. Dash and D. Sarkar, "Microstrip Patch Antenna System With Enhanced Inter-Port Isolation for Full-Duplex/MIMO Applications," *IEEE Access*, vol. 9, pp. 156222–156228, 2021, <https://doi.org/10.1109/ACCESS.2021.3128997>.
- [5] M. O. Dwairi, "Increasing Gain Evaluation of 2x1 and 2x2 MIMO Microstrip Antennas," *Engineering, Technology & Applied Science Research*, vol. 11, no. 5, pp. 7531–7535, Oct. 2021, <https://doi.org/10.48084/etasr.4305>.

- [6] S. Dey, S. Dey, and S. K. Koul, "Isolation Improvement of MIMO Antenna Using Novel EBG and Hair-Pin Shaped DGS at 5G Millimeter Wave Band," *IEEE Access*, vol. 9, pp. 162820–162834, 2021, <https://doi.org/10.1109/ACCESS.2021.3133324>.
- [7] L. Cui, J. Guo, Y. Liu, and C.-Y.-D. Sim, "An 8-Element Dual-Band MIMO Antenna with Decoupling Stub for 5G Smartphone Applications," *IEEE Antennas and Wireless Propagation Letters*, vol. 18, no. 10, pp. 2095–2099, Jul. 2019, <https://doi.org/10.1109/LAWP.2019.2937851>.
- [8] M. Li and S. Cheung, "Isolation Enhancement for MIMO Dielectric Resonator Antennas Using Dielectric Superstrate," *IEEE Transactions on Antennas and Propagation*, vol. 69, no. 7, pp. 4154–4159, Jul. 2021, <https://doi.org/10.1109/TAP.2020.3044683>.
- [9] M. Li, M. Y. Jamal, L. Jiang, and K. L. Yeung, "Isolation Enhancement for MIMO Patch Antennas Sharing a Common Thick Substrate: Using a Dielectric Block to Control Space-Wave Coupling to Cancel Surface-Wave Coupling," *IEEE Transactions on Antennas and Propagation*, vol. 69, no. 4, pp. 1853–1863, Apr. 2021, <https://doi.org/10.1109/TAP.2020.3026897>.
- [10] H. Lin, Q. Chen, Y. Ji, X. Yang, J. Wang, and L. Ge, "Weak-Field-Based Self-Decoupling Patch Antennas," *IEEE Transactions on Antennas and Propagation*, vol. 68, no. 6, pp. 4208–4217, Jun. 2020, <https://doi.org/10.1109/TAP.2020.2970109>.
- [11] T. Pei, L. Zhu, J. Wang, and W. Wu, "A Low-Profile Decoupling Structure for Mutual Coupling Suppression in MIMO Patch Antenna," *IEEE Transactions on Antennas and Propagation*, vol. 69, no. 10, pp. 6145–6153, Jul. 2021, <https://doi.org/10.1109/TAP.2021.3098565>.
- [12] N. O. Parchin *et al.*, "Eight-Element Dual-Polarized MIMO Slot Antenna System for 5G Smartphone Applications," *IEEE Access*, vol. 7, pp. 15612–15622, 2019, <https://doi.org/10.1109/ACCESS.2019.2893112>.
- [13] W. Wang and Y. Zheng, "Wideband Gain Enhancement of a Dual-Polarized MIMO Vehicular Antenna," *IEEE Transactions on Vehicular Technology*, vol. 70, no. 8, pp. 7897–7907, Dec. 2021, <https://doi.org/10.1109/TVT.2021.3094879>.
- [14] S. Yang, L. Liang, W. Wang, Z. Fang, and Y. Zheng, "Wideband Gain Enhancement of an AMC Cavity-Backed Dual-Polarized Antenna," *IEEE Transactions on Vehicular Technology*, vol. 70, no. 12, pp. 12703–12712, Sep. 2021, <https://doi.org/10.1109/TVT.2021.3119643>.
- [15] Z. Akhter, R. M. Bilal, and A. Shamim, "A Dual Mode, Thin and Wideband MIMO Antenna System for Seamless Integration on UAV," *IEEE Open Journal of Antennas and Propagation*, vol. 2, pp. 991–1000, 2021, <https://doi.org/10.1109/OJAP.2021.3115025>.
- [16] Z. Chen, W. Zhou, and J. Hong, "A Miniaturized MIMO Antenna With Triple Band-Notched Characteristics for UWB Applications," *IEEE Access*, vol. 9, pp. 63646–63655, 2021, <https://doi.org/10.1109/ACCESS.2021.3074511>.
- [17] G. Kim and S. Kim, "Design and Analysis of Dual Polarized Broadband Microstrip Patch Antenna for 5G mmWave Antenna Module on FR4 Substrate," *IEEE Access*, vol. 9, pp. 64306–64316, 2021, <https://doi.org/10.1109/ACCESS.2021.3075495>.
- [18] H. Alsaif, "Extreme Wide Band MIMO Antenna System for Fifth Generation Wireless Systems," *Engineering, Technology & Applied Science Research*, vol. 10, no. 2, pp. 5492–5495, Apr. 2020, <https://doi.org/10.48084/etasr.3413>.
- [19] P. Bora, P. Pokkunuri, and B. T. P. Madhav, "The Design of Closed Square RR Loaded 2-Port MIMO for Dual Band Applications," *Engineering, Technology & Applied Science Research*, vol. 12, no. 2, pp. 8382–8387, Apr. 2022, <https://doi.org/10.48084/etasr.4760>.
- [20] S. S. Sarade and S. D. Ruikar, "A Different Shaped Radiating Element Wide Band Multi-Band Massive MIMO Antenna for 5G/WLAN applications with Enhanced Correlation Coefficient," *IOP Conference Series: Materials Science and Engineering*, vol. 1187, no. 1, p. 012017, Jun. 2021, <https://doi.org/10.1088/1757-899X/1187/1/012017>.
- [21] C. A. Balanis, *Antenna Theory: Analysis and Design*, 3rd ed. Hoboken, N.J, USA: Wiley, 2005.